New formulation of the two-dimensional steep-slope shallow water equations. Part I: Theory and analysis

New formulation of the two-dimensional steep-slope shallow water equations. Part I: Theory and analysis

Andrea Maranzoni [a,]*, Massimo Tomirotti [b]

[a] *Department of Engineering and Architecture, University of Parma, Parco Area delle Scienze 181/A, 43124 Parma, Italy*

[b] *Department of Civil, Environmental, Architectural Engineering and Mathematics, University of Brescia, via Branze 43, 25121 Brescia, Italy*

*Corresponding author. E-mail: andrea.maranzoni@unipr.it

Abstract Two-dimensional (2D) depth-averaged shallow water equations (SWE) are widely used to model unsteady free surface flows, such as flooding processes, including those due to dam-break or levee breach. However, the basic hypothesis of small bottom slopes may be far from satisfied in certain practical circumstances, both locally at geometric singularities and even in wide portions of the floodable area, such as in mountain regions. In these cases, the classic 2D SWE might provide inaccurate results, and the steep-slope shallow water equations (SSSWE), in which the assumption of small bottom slopes is not included, are a valid alternative modeling option. However, different 2D formulations of this set of equations can be found in the geophysical flow literature, in both global horizontally-oriented and local bottom-oriented coordinate systems. In this paper, a new SSSWE model is presented in which water depth is defined along the vertical direction and flow velocity is assumed parallel to the bottom surface. This choice of the dependent variables combines the advantages of considering the flow velocity parallel to the bottom, as can be expected in gradually varied shallow flow, and handling vertical water depths consistent with elevation data, usually available as digital terrain models. The pressure distribution is assumed linear along the vertical direction and flow curvature effects are neglected. A new formulation of the 2D depth-averaged shallow water equations on steep bottom slopes is derived, in which the two dynamic equations represent momentum balances along two spatial directions parallel to the bottom, whose horizontal projections are parallel to two fixed orthogonal coordinate directions. The analysis of the mathematical properties of the new SSSWE equations shows that they are strictly hyperbolic for wet bed conditions and reduce to the conventional 2D SWE when bottom slopes are small. Finally, it is shown that the SSSWE predict a slower flow compared with the conventional SWE in the theoretical case of a 1D dam-break on a frictionless channel with fixed slope. The capabilities of the proposed model are demonstrated

in a companion paper on the basis of numerical and experimental tests.

Highlights

- A new formulation of the 2D depth-averaged shallow water equations on steep bottom slopes is presented.
- Water depth is measured vertically and velocity is assumed parallel to the bottom surface.
- The momentum equations represent linear momentum balance along two directions parallel to the bottom, which are in general non-orthogonal on irregular topography.
- The effect of steep bottom slopes on vertical pressure distribution is taken into account.
- The proposed equations are hyperbolic and reduce to the conventional 2D shallow water equations when bottom slopes are small.

Keywords Basic flow equations; Free surface flow; Shallow water equations; Steep bottom slopes; Two-dimensional depth-averaged model.

1. Introduction

The two-dimensional (2D) depth-averaged free surface flow equations under the shallow water approximation are a standard mathematical model widely used to describe a variety of gravity-driven geophysical flow phenomena, including flooding due to dam-break (e.g. Aureli et al., 2008; Wang et al., 2011; Petaccia and Natale, 2020; Pilotti et al., 2020) or levee breach (e.g., Viero et al., 2013; Dazzi et al., 2019; D'Oria et al., 2019), overland flows (e.g. Singh et al., 2015; Cea and Bladé, 2015; Costabile et al., 2020), mixed free surface-pressurized flows (Maranzoni et al., 2015; Maranzoni and Mignosa, 2018; Cea and López-Núñez, 2021), tsunami propagation and inundation of coastal regions (e.g. Segur, 2007; LeVeque et al., 2011), tidal bore propagation in river estuaries (e.g. Pan et al., 2007), atmospheric air currents over non-flat terrain (Sivakumaran and Dressler, 1989) and, based on the continuum mechanics approach, even granular flows (e.g. Denlinger and Iverson, 2004; Mangeney-Castelnau et al., 2005; Juez et al., 2013; Castro-Orgaz et al., 2015) and snow avalanches (e.g. Christen et al., 2010; Barbolini et al., 2000), as well as flows of fluid-sediment mixtures, such as debris or mud flows (e.g. Han and Wang, 1996; Laigle and Coussot, 1997; Rickenmann et al. 2006). In all these application fields, despite the limitations connected to the basic restrictive assumptions (e.g. Basco, 1989; Hu and Meyer, 2005; Van Emelen et al., 2014) and the difficulties related to the calibration of the model parameters (e.g. Barbolini et al., 2000; Guinot and Cappelaere, 2009), the 2D depth-averaged shallow water model is generally

accepted to be capable to predict the main flow features for flood hazard assessment and flood risk management (e.g. O'Brien et al., 1993; Nakagawa and Takahashi, 1997; Aureli et al., 2006; Rickenmann et al. 2006; Gruber and Bartelt, 2007; Xia et al., 2011; D'Oria et al., 2019). Furthermore, the use of 2D depth-averaged numerical models for free surface flow simulations is currently facilitated by the increasing availability of efficient user-oriented software (Teng et al., 2017), sometimes freeware, such as BASEMENT, HEC-RAS 2D, and TELEMAC-2D (e.g. Horritt and Bates, 2002; Zischg et al., 2018; Pilotti et al., 2020; Sharma and Regonda, 2021).

Among the key assumptions of the classic 2D depth-averaged shallow water equations (SWE), there is the hypothesis of small bottom slopes (e.g. Chow, 1959, Henderson, 1966; Toro, 2001). Bottom slopes are usually considered "small" when less than 1:10, which corresponds to inclination angles less than approximately 6° (Chow, 1959; p. 33). According to this hypothesis, the bottom surface can be considered practically horizontal and the flow depth can be indifferently measured along the vertical direction or the direction normal to the bottom; the flow velocity, which is assumed uniform on the vertical depth, is represented by two orthogonal horizontal components. Since the vertical component of the fluid acceleration can be neglected in comparison with gravity according to the shallow water approximation, the pressure distribution is essentially hydrostatic in the vertical direction (Acheson, 1990; Toro, 2001; Castro-Orgaz and Hager, 2017).

However, the topography on which free surface flows occur is sometimes very steep and irregular, with slopes greater than 1:10, such as in mountain regions or, locally, near geometric singularities. In these contexts, the small bottom slope assumption is violated and the classic depth-averaged SWE are no longer strictly valid. Firstly, the vertical component of the fluid acceleration can be non-negligible, thereby significantly affecting the physical process and inducing three-dimensional effects (e.g. Aureli et al., 2015; Horna-Munoz and Constantinescu, 2020). Then, the pressure distribution is non-hydrostatic along the vertical (Juez et al., 2013; Castro-Orgaz and Hager, 2017). Nevertheless, 1D and 2D SWE are commonly used in flood hazard analysis, even in the presence of steep and deeply irregular topographies (e.g. Han and Wang, 1996; Valiani et al., 2002; Begnudelli and Sanders, 2007; Aureli et al., 2008; Pilotti et al., 2011; Wang et al. 2011; de Almeida et al., 2012; Aureli et al., 2014; Pilotti et al., 2014; Touma and Kanbar, 2018). The vertical pressure distribution is non-hydrostatic also where flow curvature is significant; in this case, a depth-averaged Boussinesq-type model could be used (e.g. Castro-Orgaz et al., 2015; Cantero-Chinchilla et al., 2016; Castro-Orgaz and Hager, 2017, cap. 2; Fabiani and Ota, 2019; Cantero-Chincilla et

al., 2020). However, these higher-order effects are not considered in this paper.

For flows on steep topographies, the steep-slope shallow water equations (SSSWE) could be considered as a valid modeling option because the effect of steep bottom slopes is included (i.e. the restrictive hypothesis of small bottom slopes is removed), maintaining the assumption of negligible fluid acceleration normal to the bottom). In the one-dimensional (1D) framework, there is general agreement on the formulation of the SSSWE, based on a local bottom-oriented coordinate system following the fixed shape of the channel bottom. In this local coordinate system, the longitudinal axis is parallel to the bottom and the other axis is normal to it. Consistently, flow velocity is assumed parallel to the channel bottom and flow depth is defined orthogonally to it. In the resulting equations, representing mass conservation and momentum balance along the sloping flow direction, the effect of the bottom slope is included in both pressure and bottom terms, in which trigonometric functions of the bed inclination angle appear (e.g. Berger, 1994; Fernandez-Feria, 2006; Takahashi, 2007; Ancey et al., 2008; Van Emelen et al., 2014). This approach is systematically adopted in 1D modeling of both flows in steep channels with fixed bottom slope (e.g. Savage and Hutter, 1989; Berger, 1994; Keller, 2003; Fernandez-Feria, 2006; Ancey et al., 2008; Antuono and Hogg, 2009) and curvilinear flows in channels with curved bottom (e.g. Dressler, 1978; Castro-Orgaz and Hager, 2014; Castro-Orgaz and Hager, 2016).

Conversely, various 2D formulations of the SSSWE have been proposed in the wide gravity-driven flow literature, although such equations always represent the basic principles of mass conservation and linear momentum balance in the 2D context. The discrepancies between the existing 2D formulations are mainly due to the different approaches adopted in deriving the equations and the different ways of introducing the bottom slope effects. In particular, some approaches assume a local rectangular coordinate system with bottom-oriented axes – i.e. a local coordinate system following the terrain, with two axes parallel to the bottom and the third axis locally orthogonal to it – (Iverson and Denlinger, 2001; McDougall and Hungr, 2004; Medina et al., 2008; Juez et al., 2013), whereas other approaches are based on a horizontally-oriented coordinate system – i.e. a classic fixed Cartesian coordinate system, in which two axes are horizontal and the third axis is vertical and aligned with the gravity vector (Chaudhry, 1993; Laigle, 1997; Denlinger and Iverson, 2004; Rickenmann et al., 2006; Denlinger and O'Connel, 2008; Ni et al., 2019; Juez et al., 2013; Xia and Liang, 2018). In the models based on local bottom-oriented coordinates, flow depth is measured along the direction normal to the bottom and flow velocity is assumed

parallel to the local terrain surface, whereas in the models that use global horizontally-oriented coordinates, the water surface is identified by its vertical elevation above the bottom and flow velocity is described by two orthogonal horizontal components.

In the presence of steep bottom slopes, the choice of a local bottom-oriented coordinate system seems, at a first glance, better in the analysis of shallow water flows. Indeed, in quasi-parallel flows on sloping planar bottom surfaces, it is natural to assume the flow velocity parallel to the bottom surface and the flow depth normal to it. In this case, according to the shallow water approximation, the fluid acceleration component normal to the bottom is negligible and, consequently, the pressure distribution is hydrostatic on each cross-section of the flow. However, the use of a local coordinate system following the topography can cause practical problems in defining the initial condition, handling the topographic data (Juez et al., 2013; p. 203), or returning the results, since topographic information is typically available through a digital elevation model, which provides terrain elevation data with reference to a horizontal geodetic datum (Denlinger and Iverson, 2004; p. 2). For this reason, various formulations of the 2D SSSWE in global horizontally-oriented coordinates can be found in the literature, which mainly differ in how the effect of bottom slope on pressure distribution is included in the model. A comprehensive review of the 2D depth-averaged SSSWE models proposed in the literature is presented in Appendix A. It worth noting that some of these models present serious critical issues. In particular, in some proposed formulations, the pressure correction coefficient that appears in the equations to take into account the effect of steep bottom slope on vertical pressure distribution is not symmetric with respect to the exchange of the spatial coordinates (see Eqs (A1) and (A3) in Appendix A), contrary to what expected.

To combine the advantages of the two alternative approaches, this paper proposes a new formulation of the 2D SSSWE, which uses the vertical water depth, defined as the vertical distance of the water surface above the bottom, and two flow velocity components parallel to the bottom as depending variables. The independent variables are two orthogonal horizontal coordinates and time. The use of spatial (dependent or independent) variables defined with respect to a conventional horizontally-oriented Cartesian reference frame allows for efficient and direct manipulation of the data of a digital terrain model. The depth-averaged governing equations are derived by applying the basic principles of mass conservation and linear momentum balance to a vertical column of incompressible water extending from the bottom to the free surface. The pressure distribution is assumed linear (non-hydrostatic) in the vertical direction, neglecting the effects of flow curvature.

The eigenstructure and some special cases of the new set of equations are discussed in detail. Moreover, the simple case of a 1D dam-break on a frictionless sloping straight channel with fixed positive bottom slope is considered to perform a first comparison of the analytical results provided by the proposed SSSWE model and the conventional SWE model in the presence of high bottom slopes. A more extensive comparison on the basis of validation and numerical test cases will be performed in the companion paper (Maranzoni and Tomirotti, 2021), in which a finite volume numerical scheme is used to solve the equations.

This paper is organized as follows. Section 2 presents the conceptual bases of the model. The new formulation of the equations is presented in Section 3, and the mathematical properties of the equations are discussed in Section 4, along with some special cases. The 1D dam-break problem on a frictionless sloping channel with fixed slope is analyzed in Section 5. Concluding remarks are drawn in Section 6. Finally, a review of the existing formulations of the 2D SSSWE is provided in Appendix A, while detailed derivations of the equations and their eigenstructure are presented in Appendixes B and C, respectively.

2. Conceptual bases of the model

Using a local bottom-oriented coordinate system (e.g. Gray et al., 1999; Iverson and Denlinger, 2001), the shallow water equations are expressed in terms of flow depth measured normally to the bottom and depth-averaged velocity components locally parallel to the bottom.

However, defining the flow depth orthogonally to the bottom can cause some practical difficulties. For example, in Fig. 1, which sketches the initial condition of the dam-break problem in a sloping channel, straight line AA’ traced orthogonally from the bottom immediately upstream of the dam intersects the dam and does not reach the water surface. In this case, the depth of the water column does not represent correctly the water depth appearing in the equations. To overcome this problem (which, for fixed dam height, affects a longer channel stretch upstream of the dam as the bottom slope increases) and avoid the ensuing mathematical complications in the analysis of the dam-break problem (Fernandez-Feria, 2006), the dam was assumed perpendicular to the bottom in some applications (e.g. Ancey et al., 2008), although this configuration is evidently unrealistic.

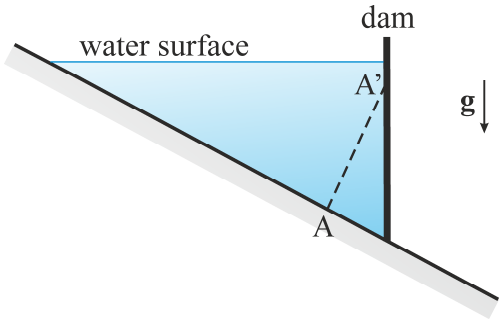

Fig. 1. Example of a difficulty that can be encountered in 1D dam-break modeling in a sloping channel considering bottom-normal flow depths: segment AA' intersects the dam (and not the water surface) and does not define correctly a water depth measured perpendicularly from the bottom.

As a further example of such practical problems, Fig. 2 shows that, when the flow has concave curvature in the longitudinal vertical plane due to the curved bottom, different straight lines traced orthogonally from the bottom can intersect before reaching the free surface (lines AA' and BB' in Fig. 2), causing an erroneous representation of the flow volume. Additionally, since topographic information is commonly available as digital elevation data, the use of flow depths measured perpendicularly from the terrain potentially requires laborious pre- and post-processing calculations for the transformation from vertical depths to normal-bottom depths and vice versa, especially on irregular topography (Denlinger and Iverson, 2004; Medina et al., 2008).

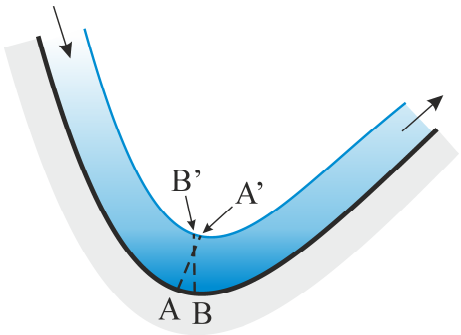

Fig. 2. Example of geometrical difficulties caused by a curved bottom: lines AA' and BB' traced orthogonally to the bottom intersect.

Given these problems, it seems reasonable to explore the possibility of modeling a shallow water flow on steep topography considering the flow depth defined along the vertical direction and the flow velocity parallel to the bottom surface. Hence, water depth, h, is

defined with reference to the *z*-axis (aligned with the vertical direction and oriented upwards) of a global fixed Cartesian frame of reference O*xyz*, while flow velocity components, *u* and *v*, are defined with reference to the ξ- and η-axis of a local bottom-oriented reference frame, Pξηζ, in which axes ξ and η identify the tangent plane that approximates locally the bottom surface at each point P and axis ζ is locally normal to the bottom surface (Fig. 3). Axes ξ and η are characterized by the property that their horizontal projections have the same directions of orthogonal horizontal axes *x* and *y* of a fixed global frame of reference O*xyz*, respectively (i.e. ξ and η directions are locally tangent to the coordinate lines corresponding to directions *x* and *y* on the bottom surface, respectively; Fig. 3b). Denoting with $\hat{\mathbf{i}}$, $\hat{\mathbf{j}}$, and $\hat{\mathbf{k}}$ the unit vectors of the *x*, *y*, and *z* axes of the global reference frame, respectively, the unit vectors of the ξ and η axes of the local reference frame with respect to the global one are respectively

$$\hat{\boldsymbol{\xi}} = \cos\theta_x \hat{\mathbf{i}} - \sin\theta_x \hat{\mathbf{k}} \quad \text{and} \quad \hat{\boldsymbol{\eta}} = \cos\theta_y \hat{\mathbf{j}} - \sin\theta_y \hat{\mathbf{k}}, \tag{1}$$

where θ_x and θ_y are the inclination angles of the bottom surface in the directions *x* and *y*, respectively. Both these angles range between –90° and 90° (excluding the extreme values) and can be easily computed from the topographic data. Unit vectors $\hat{\boldsymbol{\xi}}$ and $\hat{\boldsymbol{\eta}}$ constitute a basis for the 2D vector space on the plane locally tangent to the surface bottom in P. Moreover, axes ξ and η are in general non-orthogonal because $\hat{\boldsymbol{\xi}} \cdot \hat{\boldsymbol{\eta}} = \sin\theta_x \sin\theta_y = \cos\varphi$, where φ denotes the angle between local directions ξ and η (Fig. 3a); they are orthogonal only when either $\theta_x = 0$ or $\theta_y = 0$, or both.

The unit vector of the ζ-direction locally normal to the bottom surface at each point P can be represented in the global reference frame as

$$\hat{\boldsymbol{\zeta}} = \frac{\tan\theta_x}{\sqrt{1+\tan^2\theta_x+\tan^2\theta_y}}\hat{\mathbf{i}} + \frac{\tan\theta_y}{\sqrt{1+\tan^2\theta_x+\tan^2\theta_y}}\hat{\mathbf{j}} + \frac{1}{\sqrt{1+\tan^2\theta_x+\tan^2\theta_y}}\hat{\mathbf{k}}\,. \tag{2}$$

Accordingly, the vertical component of the $\hat{\boldsymbol{\zeta}}$-unit vector (i.e. $\hat{\boldsymbol{\zeta}} \cdot \hat{\mathbf{k}}$) is equal to the cosine of ψ, which is the angle between the direction normal to the bottom and the vertical (Fig. 3a).

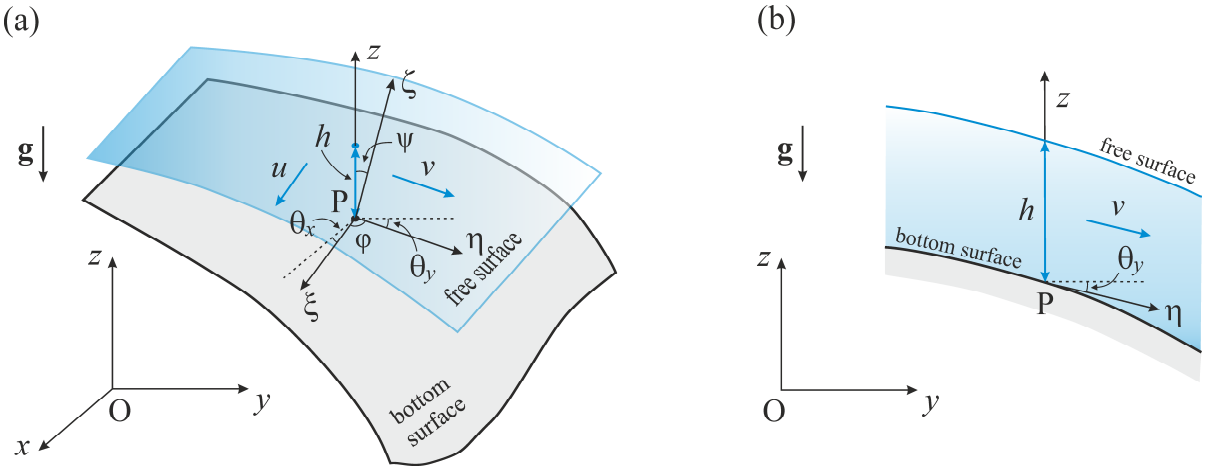

Fig. 3. Definition sketch of free-surface flow on a steep bottom surface: (a) 3D view; (b) profile view on the *yz* vertical plane.

Based on this approach, flow velocity **v** can be expressed as the sum of the two vector components $u\hat{\boldsymbol{\xi}}$ and $v\hat{\boldsymbol{\eta}}$ along the ξ and η directions, respectively, as

$$\mathbf{v} = u\hat{\boldsymbol{\xi}} + v\hat{\boldsymbol{\eta}}, \tag{3}$$

or

$$\mathbf{v} = u\cos\theta_x\hat{\mathbf{i}} + v\cos\theta_y\hat{\mathbf{j}} - (u\sin\theta_x + v\sin\theta_y)\hat{\mathbf{k}} \tag{4}$$

in the global reference frame. Consequently, the flow velocity magnitude is

$$\|\mathbf{v}\| = \sqrt{\mathbf{v}\cdot\mathbf{v}} = \sqrt{u^2 + v^2 + 2uv(\hat{\boldsymbol{\xi}}\cdot\hat{\boldsymbol{\eta}})} = \sqrt{u^2 + v^2 + 2uv\sin\theta_x\sin\theta_y}\,. \tag{5}$$

The two velocity components are assumed uniform on the vertical column of fluid, as in the 2D depth-averaged models. The *U* and *V* orthogonal projections of flow velocity **v** in the ξ and η directions, respectively, can be expressed as a function of *u* and *v* as

$$U = \mathbf{v}\cdot\hat{\boldsymbol{\xi}} = u + v\sin\theta_x\sin\theta_y \quad \text{and} \quad V = \mathbf{v}\cdot\hat{\boldsymbol{\eta}} = v + u\sin\theta_x\sin\theta_y\,. \tag{6}$$

Eq. (4) shows that the horizontal velocity components along the orthogonal *x*- and *y*-directions are respectively

$$v_x = \mathbf{v}\cdot\hat{\mathbf{i}} = u\cos\theta_x \quad \text{and} \quad v_y = \mathbf{v}\cdot\hat{\mathbf{j}} = v\cos\theta_y\,, \tag{7}$$

and that the vertical component of the flow velocity is negligible only if both θ_x and θ_y are small (i.e. the bottom is locally nearly horizontal).

Flow variables *h*, *u*, and *v* are considered to be functions of horizontal spatial coordinates *x* and *y*, as well as of time *t*, as in the conventional 2D depth-averaged SWE.

3. Governing equations

The new 2D SSSWE are derived by applying the basic principles of mass conservation and linear momentum balance to a fixed infinitesimal parallelepiped control volume bounded by vertical faces and extending from the slanted bottom surface (assumed planar and non-erodible) up to the free surface (Fig. 4). The area of the parallelogram bottom of this infinitesimal control volume is

$$dA = \left\| d\xi\,\hat{\boldsymbol{\xi}} \times d\eta\,\hat{\boldsymbol{\eta}} \right\| = d\xi\, d\eta\, \sin\varphi = d\xi\, d\eta \sqrt{1-\sin^2\theta_x \sin^2\theta_y} = d\xi\, d\eta\, \cos\theta_x \cos\theta_y \sqrt{1+\tan^2\theta_x + \tan^2\theta_y}\,, \tag{8}$$

where $d\xi$ and $d\eta$ are the lengths of the sides of the bottom face, and symbol "×" denotes the vector product. Hence, the area of the horizontal projection (on the *xy*-plane) of the bottom of the control volume is

$$d\Omega = dA\,\hat{\boldsymbol{\zeta}} \cdot \hat{\mathbf{k}} = d\xi\, d\eta \sin\varphi \cos\psi = d\xi\, d\eta\, \cos\theta_x \cos\theta_y = dx\, dy \tag{9}$$

in view of the geometric relations

$$dx = d\xi \cos\theta_x \quad \text{and} \quad dy = d\eta \cos\theta_y\,. \tag{10}$$

The vertical orientation of the control volume prevents superimpositions or distortions (Mancarella and Hungr, 2010), especially in curvilinear flows in the vertical plane (Fig. 2), allowing the lateral faces of adjacent control volumes to match (Denlinger and Iverson, 2004).

The momentum equations represent linear momentum balance along the inclined ξ- and η-directions, consistently with the hypothesis of flow velocity locally parallel to the bottom surface. The model is applied to incompressible inviscid water flow, thus considering an isotropic stress tensor and neglecting internal viscous and turbulent stresses. According to the assumption of gradually varied flow, the pressure distribution is assumed linear on the lateral faces of the control volume, neglecting the effect of flow curvature.

Details on the derivation of the equations are reported in Appendix B.

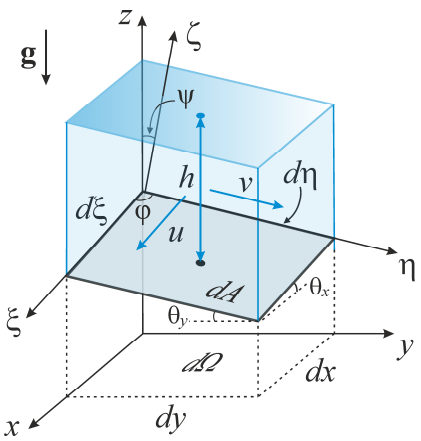

Fig. 4. Infinitesimal control volume used for the derivation of the 2D vertically-averaged equations.

The vertically-averaged governing equations can be written in conservative form as

$$\frac{\partial \mathbf{U}}{\partial t}+\frac{\partial \mathbf{F}}{\partial x}+\frac{\partial \mathbf{G}}{\partial y}=\mathbf{S} \tag{11}$$

with

$$\mathbf{U}=\begin{bmatrix} h \\ Uh \\ Vh \end{bmatrix},\ \mathbf{F}=\begin{bmatrix} uh\cos\theta_x \\ \left(uUh+\frac{1}{2}kgh^2\right)\cos\theta_x \\ uVh\cos\theta_x \end{bmatrix},\ \mathbf{G}=\begin{bmatrix} vh\cos\theta_y \\ Uvh\cos\theta_y \\ \left(vVh+\frac{1}{2}kgh^2\right)\cos\theta_y \end{bmatrix},\ \mathbf{S}=\begin{bmatrix} 0 \\ gh(S_{0\xi}-S_{f\xi}) \\ gh(S_{0\eta}-S_{f\eta}) \end{bmatrix}, \tag{12}$$

in which **U** is the vector of conserved variables (i.e. the vertical depth, h, and the Uh and Vh unit discharges in the ξ- and η-direction, respectively), **F** and **G** are the vectors of physical fluxes, and **S** is the source term; g is the gravity acceleration and k (≤ 1) a pressure correction factor. The bottom slopes are

$$S_{0\xi}=\sin\theta_x \quad \text{and} \quad S_{0\eta}=\sin\theta_y \tag{13}$$

in the ξ- and η-direction, respectively, and the friction slopes along the same directions are

$$S_{f\xi}=\frac{n^2u\|\mathbf{v}\|}{h^{4/3}}\sqrt{1+\tan^2\theta_x+\tan^2\theta_y} \quad \text{and} \quad S_{f\eta}=\frac{n^2v\|\mathbf{v}\|}{h^{4/3}}\sqrt{1+\tan^2\theta_x+\tan^2\theta_y}\,, \tag{14}$$

where n is the Manning roughness coefficient.

In Eq (12), k describes the effect of bottom slope on vertical pressure distribution. Actually, for a parallel flow in a straight open channel of slope angle θ, this distribution is no longer hydrostatic and the pressure head at a vertical transverse section is equal to the vertical depth multiplied by the corrector factor $\cos^2\theta$, as shown by Chow (1959, p. 33) and Henderson (1966, p. 28). This result also applies approximately to gradually varied flows and

can be generalized to the 2D case setting

$$k = \begin{cases} 1 & \text{if } \|\mathbf{v}\| = 0 \\ \cos^2 \psi = \dfrac{1}{1 + \tan^2 \theta_x + \tan^2 \theta_y} & \text{otherwise} \end{cases}. \tag{15}$$

According to Eq. (15), the pressure correction factor is set to unity in static conditions (when the pressure distribution is hydrostatic), while, in dynamic conditions, k is assumed equal to the square cosine of the angle between the direction locally normal to the bottom and the vertical ~~flow direction and its horizontal projection~~ (Juez et al., 2013; Xia and Liang, 2018; Ni et al., 2019). Over non-horizontal bottom (i.e. $\theta_x \neq 0$ and $\theta_y \neq 0$), k is discontinuous for $\|\mathbf{v}\| \to 0^+$; actually, according to the assumption that flow velocity is parallel to the bottom surface, the vertical pressure distribution changes abruptly from hydrostatic as soon as the flow motion starts. In the special case of a unidirectional uniform flow in a sloping channel with fixed slope in the longitudinal ξ-direction (i.e. θ_x = const., θ_y =0), $\psi = \theta_x$ and k reduces to $\cos^2\theta_x$, as expected. In particular, for θ_x tending to 90°, k tends to 0, which is representative of a free falling fluid with the vertical pressure gradient equal to zero (Denlinger and Iverson, 2004; p. 4). In a 2D flow on small bottom slopes (i.e. $\theta_x \cong 0$ and $\theta_y \cong 0$), the value of k does not differ appreciably from unity and the pressure terms in Eq. (12) become practically of hydrostatic type, as in the classic SWE. Finally, it is worth noting that, based on the definition of Eq. (15), k is symmetric with respect to the two horizontal directions x and y, because θ_x and θ_y are interchangeable. To take into account the effects of streamline curvature on pressure distribution, a further correction factor could be introduced in the pressure term (Chow, 1959; p. 33). However, when the effect of curvature is significant, such as in flows over curved bottom or flows with strongly curved water surface on even topography, Boussinesq-type equations provide more accurate predictions since non-linear terms are added to the conventional hydrostatic pressure term (e.g. Basco, 1989; Mohapatra and Chaudhry, 2004; Kim and Lynett, 2011, Cantero-Chinchilla et al., 2016, Castro-Orgaz and Hager, 2017).

In Eqs (11)–(12), dependent flow variables Uh and Vh are defined in terms of vertically-averaged velocity components U and V. However, velocity components u and v also appear in the flux vectors. Inverting Eq. (6), velocities components u and v can be calculated from U and V as

$$u = \frac{U - V \sin\theta_x \sin\theta_y}{1 - \sin^2\theta_x \sin^2\theta_y} = \frac{U - V\cos\varphi}{\sin^2\varphi}, \qquad v = \frac{V - U \sin\theta_x \sin\theta_y}{1 - \sin^2\theta_x \sin^2\theta_y} = \frac{V - U\cos\varphi}{\sin^2\varphi}. \tag{16}$$

The new SSSWE [Eqs (11)–(12)] present four main differences compared with the conventional SWE: i) the flux terms depend on the local bottom slope through inclination angles θ_x and θ_y; ii) a correction factor, which reduces the gravity effect, appears in the pressure term; this factor depends only on the local bottom slope; iii) the bottom source term is expressed as a function of the sine (and not of the tangent) of bottom inclination angles θ_x and θ_y; actually, the sine of an angle cannot be approximated with its tangent when the angle is not small; iv) friction stresses act on a bottom surface that is significantly larger than its horizontal projection for steep topographies and the friction term depends on the bottom slope.

4. Properties of the equations

4.1 Hyperbolicity

The character of the new equations can be determined by analyzing the eigenstructure of their homogeneous form in terms of the conserved variables (Toro, 2001). This analysis is reported in Appendix C, where it is shown that the equations are strictly hyperbolic for a wet bed.

Wave celerity is different in the two directions ξ and η, and varies with the local bottom inclination and flow velocity, as well as the vertical flow depth (Eqs (C4) and (C5) in Appendix C). Single elementary waves of small amplitude propagating in quiescent water ($k = 1$) over non-flat steep topography move with speed

$$c_\xi = \sqrt{gh}\,\frac{\cos\theta_x}{\sin\varphi} \quad \text{and} \quad c_\eta = \sqrt{gh}\,\frac{\cos\theta_y}{\sin\varphi} \tag{17}$$

in the ξ- and η-direction, respectively. For a 1D flow in the ξ-direction in a sloping channel of fixed slope (i.e. $\theta_x = \text{const}$, $\theta_y = 0$, and $\varphi = 90°$), the wave celerity is

$$c_\xi = \sqrt{gh}\,\cos\theta_x = \sqrt{g\cos^2\theta_x h}\ , \tag{18}$$

in which the gravity acceleration is corrected by the reduction coefficient $\cos^2\theta_x$, dependent only on the channel slope (Van Emelen et al., 2014). In the limit case of small bottom slopes, both c_ξ and c_η in Eq. (17) reduce to $(gh)^{1/2}$, which is the wave celerity in the conventional 2D SWE.

4.2 Special cases

The new set of equations reduces to the conventional 2D SWE if bottom slopes are small (i.e. $\theta_x \cong \theta_y \cong 0$, and consequently $\cos\theta_x \cong \cos\theta_y \cong 1$, $\sin\theta_x \cong \tan\theta_x$, $\sin\theta_y \cong \tan\theta_y$, and $k = 1$).

This simplification is obtained automatically in the regions of the flow domain where the topography is flat with gentle slopes.

In the special case of 2D flow spreading on an inclined plane in which ξ is the coordinate along the direction of maximum slope (i.e. θ_x = const and $\theta_y = 0$; consequently, $\varphi = 90°$ and $\psi = \theta_x$), U and V are respectively equal to u and v in view of Eq. (6), and the system of equations (11)–(12) become

$$\begin{cases} \dfrac{\partial h}{\partial t} + \dfrac{\partial (uh\cos\theta_x)}{\partial x} + \dfrac{\partial (vh)}{\partial y} = 0 \\ \dfrac{\partial (uh)}{\partial t} + \dfrac{\partial}{\partial x}\left[\left(u^2 h + \dfrac{1}{2}kgh^2\right)\cos\theta_x\right] + \dfrac{\partial}{\partial y}(uvh) = gh\left(\sin\theta_x - \dfrac{n^2 u\|\mathbf{v}\|}{h^{4/3}}\sqrt{1+\tan^2\theta_x}\right) \\ \dfrac{\partial (vh)}{\partial t} + \dfrac{\partial}{\partial x}(uvh\cos\theta_x) + \dfrac{\partial}{\partial y}\left(v^2 h + \dfrac{1}{2}kgh^2\right) = gh\left(-\dfrac{n^2 v\|\mathbf{v}\|}{h^{4/3}}\sqrt{1+\tan^2\theta_x}\right) \end{cases} \tag{19}$$

with

$$k = \begin{cases} 1 & \text{if } \|\mathbf{v}\| = 0 \\ \cos^2\theta_x & \text{otherwise} \end{cases}. \tag{20}$$

The associated 1D ξ-split equations (i.e. $v = 0$) of unsteady flow in a wide rectangular channel of fixed slope θ_x are

$$\begin{cases} \dfrac{\partial h}{\partial t} + \dfrac{\partial (uh\cos\theta_x)}{\partial x} = 0 \\ \dfrac{\partial (uh)}{\partial t} + \dfrac{\partial}{\partial x}\left[\left(u^2 h + \dfrac{1}{2}kgh^2\right)\cos\theta_x\right] = gh\left(\sin\theta_x - \dfrac{n^2 u^2}{h^{4/3}}\sqrt{1+\tan^2\theta_x}\right) \end{cases} \tag{21}$$

with k again expressed by Eq. (20). These equations are equivalent to the classic 1D SSSWE in bottom-oriented coordinates (e.g. Berger, 1994; Ancey et al., 2008; Van Emelen et al., 2014), as can be verified by using elementary trigonometric transformations.

Finally, the new SSSWE correctly represent the special case of the static condition. Indeed, in this case, $u = v = 0$ and $k = 1$; then, Eqs (11)–(12) reduce to

$$\begin{cases} \dfrac{\partial h}{\partial t} = 0 \\ \dfrac{\partial h}{\partial x} = \tan\theta_x \\ \dfrac{\partial h}{\partial y} = \tan\theta_y \end{cases}, \tag{22}$$

as expected in static conditions, because the water surface is stationary and horizontal.

5. 1D dam-break problem in a sloping channel

Let us consider the dam-break problem in a frictionless rectangular channel of fixed bottom slope (Fig. 5). In this case, the proposed SSSWE appear as in the form of Eq. (25) without the friction term ($n = 0$). These equations can be recast in a convenient dimensionless form to obtain general solutions regardless of the value of the scaling variables (e.g. Ancey et al., 2008; Aureli et al., 2014; Maranzoni and Mignosa, 2019).

Using the dimensionless variables (denoted by an upper tilde)

$$\widetilde{x} = \frac{x}{h_0}\mathrm{tg}\theta_x, \quad \widetilde{t} = t\sqrt{\frac{g}{h_0}}\sin\theta_x, \quad \widetilde{h} = \frac{h}{h_0}\cos^2\theta_x, \quad \widetilde{u} = \frac{u}{\sqrt{gh_0}}, \tag{23}$$

where h_0 is the initial water depth at the dam location, the dimensionless equations reads

$$\begin{cases} \dfrac{\partial\widetilde{h}}{\partial\widetilde{t}} + \dfrac{\partial(\widetilde{u}\widetilde{h})}{\partial\widetilde{x}} = 0 \\ \dfrac{\partial(\widetilde{u}\widetilde{h})}{\partial\widetilde{t}} + \dfrac{\partial}{\partial\widetilde{x}}\left(\widetilde{u}^2\widetilde{h} + \dfrac{1}{2}\widetilde{h}^2\right) = \widetilde{h} \end{cases}, \tag{24}$$

Equations (24) are identical to those obtained nondimensionalizing the conventional 1D x-split SWE with the dimensionless variables (Aureli et al., 2014)

$$\widetilde{x} = \frac{x}{h_0}\mathrm{tg}\theta_x, \quad \widetilde{t} = t\sqrt{\frac{g}{h_0}\mathrm{tg}\theta_x}, \quad \widetilde{h} = \frac{h}{h_0}, \quad \widetilde{u} = \frac{u}{\sqrt{gh_0}}. \tag{25}$$

Accordingly, the analysis of the dam-break problem in a sloping channel of fixed slope performed on the basis of the SSSWE can be transformed, by proper nondimensionalization, into the analysis of a dam-break problem in the conventional SWE framework.

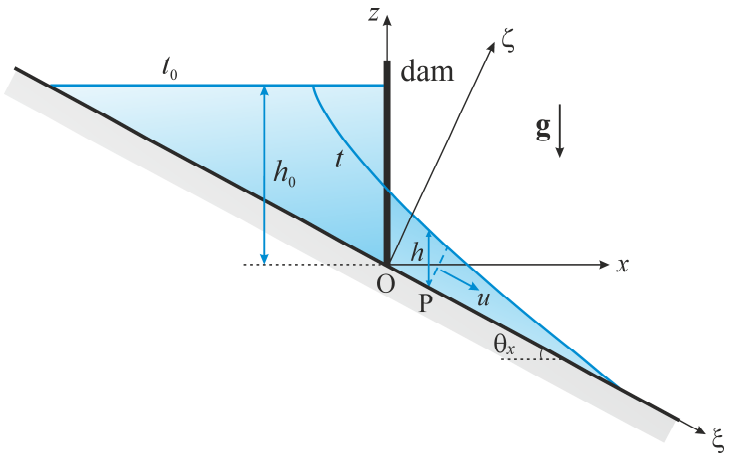

Fig. 5. 1D dam-break problem in a sloping channel with fixed bottom slope: initial condition (at time $t_0 = 0$) and water surface profile at generic time $t > 0$.

Hunt (1987) analyzed this problem using the characteristic form of the classic SWE and obtained analytically the solution domain boundaries in the dimensional *x*-*t* plane. These boundaries were obtained in dimensionless form by Dressler (1958), and later by Ancey et al. (2008) and Aureli et al. (2014) exploiting the dimensionless characteristic formulation of the equations:

$$\begin{cases} \tilde{u} + 2\tilde{c} - \tilde{t} = \text{const.} \;\; \text{along the C}_+ \text{ characteristic curve} \;\; \dfrac{d\tilde{x}}{d\tilde{t}} = \tilde{u} + \tilde{c} \\ \tilde{u} - 2\tilde{c} - \tilde{t} = \text{const.} \;\; \text{along the C}_- \text{ characteristic curve} \;\; \dfrac{d\tilde{x}}{d\tilde{t}} = \tilde{u} - \tilde{c} \end{cases}, \tag{26}$$

where $\tilde{c} = (\tilde{h})^{1/2}$ is the dimensionless wave celerity. In the dimensionless $\tilde{x}$-$\tilde{t}$ plane, the quiet front (which identify the position, as a function of time, of the tail of the rarefaction wave generated by the dam removal) is given by

$$\tilde{x}_{\text{q}}(\tilde{t}) = \frac{\tilde{t}^2}{4} - \tilde{t} \quad \text{for } 0 \le \tilde{t} \le 2\,; \tag{27}$$

the drying front (i.e. the trailing edge of the dam-break wave) is given by

$$\tilde{x}_{\text{d}}(\tilde{t}) = \frac{1}{2}(\tilde{t} - 2)^2 - 1 \quad \text{for } \tilde{t} \ge 2\,; \tag{28}$$

and the wetting front (i.e. the leading edge of the dam-break wave) is given by

$$\tilde{x}_{\text{w}}(\tilde{t}) = \frac{1}{2}(\tilde{t} + 2)^2 - 2 \quad \text{for } \tilde{t} \ge 0\,. \tag{29}$$

These boundaries are shown in Fig. 6a in the dimensionless $\tilde{x}$-$\tilde{t}$ plane.

Dimensionless Eqs (27)–(29) can then be converted into different dimensional equations for the two SSSWE and SWE models by applying the corresponding variable transformations (Eq. (23) or Eq. (25), respectively). The SSSWE and SWE solutions substantially coincide when the bottom slope is small (i.e $\cos\theta_x \cong 1$ and $\sin\theta_x \cong \tan\theta_x$).

For example, Fig. 6b compares the boundaries of the two solution domains in the *x*-*t* plane for $\theta_x = 45°$ and $h_0 = 1$ m. It can be observed that, on the whole, the standard SWE predict a faster propagation of the dam-break wave compared to the SSSWE. Indeed, the scaling time of the SWE model (Eq. 25) is less than that of the SSSWE model (Eq. 23) by a factor of $\cos\theta_x$. Accordingly, the times predicted by the conventional SWE model (e.g. the arrival time of the rarefaction wave at a selected section upstream of the reservoir; the emptying time of the reservoir; the arrival time of the dam-break wave at a selected downstream location) are shorter than the ones predicted by the SSSWE model, and the difference increases with the channel slope. The absolute percentage deviation between the two time predictions (with reference to the SSSWE one) is $100\%(1 - \cos\theta_x)$; for $\theta_x = 45°$, it reaches approximately 30%.

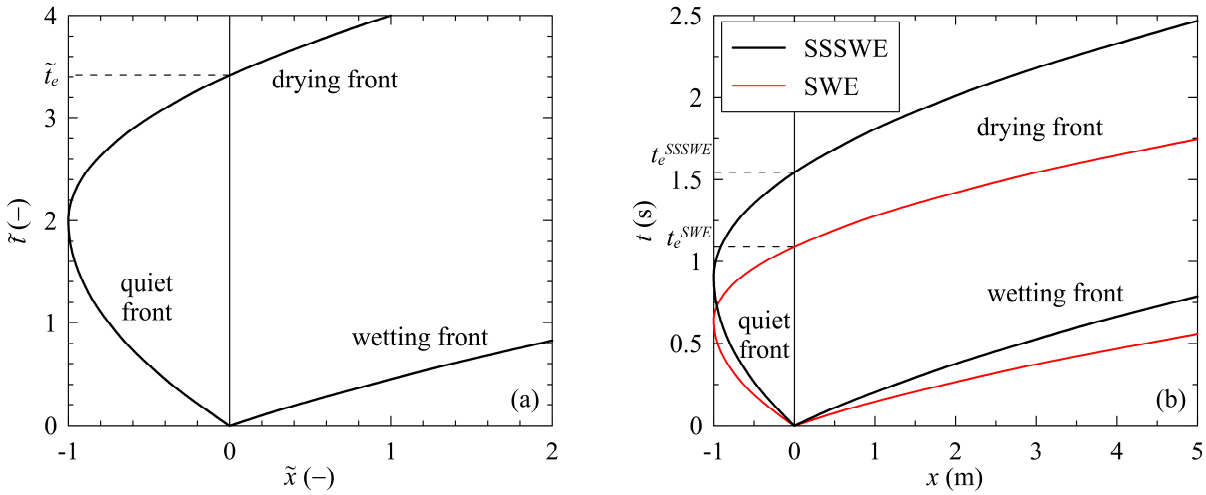

Fig. 6. Dam-break on a steep frictionless channel with fixed slope: (a) analytical solutions for the quiet front, drying front, and wetting front in the dimensionless characteristic plane; (b) comparison between the analytical solutions of the quiet, drying, and wetting fronts for the SSSWE and SWE models for $\theta_x = 45°$ and $h_0 = 1$ m. t_e denotes the empting time of the reservoir.

6. Conclusions

In this paper, a new formulation of the 2D SSSWE for unsteady water flow on steep topography has been proposed, in which flow depth is defined along the vertical direction and flow velocity is assumed locally parallel to the bottom surface. This novel approach combines the advantages of considering two velocity components parallel to the bottom (which is consistent with the 2D modeling of a quasi-parallel shallow flow) and a vertical water depth (which avoids laborious pre- and post-processing computations on elevation data).

The equations were derived from differential analysis by applying the mass conservation and linear momentum principles to an infinitesimal vertical column of water and were written in conservative vector form. According to the gradually varied flow assumption, pressure was assumed to vary linearly on the vertical depth and a correction factor was introduced to take into account the effect of bottom slope on pressure distribution. The effects of flow curvature were neglected.

The new SSSWE appear to be structurally similar to the conventional SWE but differ from them in four main respects: i) the flux terms depend on the local bottom slope; ii) a correction factor reducing the gravity effect and depending only on the local bottom topography is applied to the pressure term; iii) the bottom source term is a function of the sine of the bottom inclination angles; iv) the friction term depends on the local bottom slope.

The analysis of the eigenstructure of the new system of equations has shown that it is strictly hyperbolic for wet bed conditions, and therefore it constitutes a nonlinear hyperbolic system of conservation laws with source term, as the conventional SWE. Accordingly, the wide variety of numerical methods proposed in literature to solve this type of equations can be usefully employed in the numerical applications. Moreover, when bottom slopes are small, the new set of equations reduces to the conventional system of 2D SWE.

For a 1D dam-break flow in a frictionless sloping channel of fixed slope, both SSSWE and conventional SWE can be recast in the same dimensionless form by using different sets of dimensionless variables. This allows the analytical solutions obtained in dimensionless form from the conventional SWE model to be transferred to the SSSWE one. The comparison between the solution domains (bounded by the quiet, drying and wetting fronts) has shown that the SSSWE predict a slower dam-break wave propagation compared with the conventional SWE. This difference becomes more significant as the channel slope increases.

Ultimately, the new system of equations constitutes a shallow water model that, involving slightly more complex mathematical expressions than the conventional 2D SWE, can be considered for the 2D numerical simulation of unsteady free-surface flows on steep topography and for assessing the effect of bottom slope on the flow.

In the companion paper, this model will be solved by a finite volume numerical scheme and validated against experimental data available in the literature. The effect of steep bottom slopes will be assessed by comparing the numerical results of the SSSWE with those provided by the conventional SWE.

Appendix A – Existing formulations of the 2D SSSWE

Various formulations of the 2D SSSWE have been proposed in the literature for geophysical flows on steep bottom slopes, ranging from water flows to flows of sediment-fluid mixtures, up to granular avalanches. To easily compare different formulations, in this review the friction term is disregarded and the velocity-distribution correction coefficients are assumed equal to unity; moreover, the terms representing the effects of tangential or solid internal stresses in granular flow modeling are omitted. Accordingly, equations used in different contexts can be consistently compared.

One of the first formulations of the 2D SSSWE can be found in Chaudhry (1993; p. 352). Starting from equations expressed in a local bottom-oriented rectangular coordinate system, the author derived the following equations in global horizontal-oriented coordinates by applying a rigid rotation of the axes and introducing some simplifying assumptions:

$$\begin{cases} \dfrac{\partial h}{\partial t}+\dfrac{\partial (uh)}{\partial x}+\dfrac{\partial (vh)}{\partial y}=0 \\ \dfrac{\partial (uh)}{\partial t}+\dfrac{\partial }{\partial x}(u^2h)+gh(\cos\alpha_x\cos\alpha_z)^2\dfrac{\partial h}{\partial x}+\dfrac{\partial }{\partial y}(uvh)=gh\cos\alpha_x\sin\alpha_x \\ \dfrac{\partial (vh)}{\partial t}+\dfrac{\partial }{\partial x}(uvh)+\dfrac{\partial }{\partial y}(v^2h)+gh(\cos\alpha_y\cos\alpha_z)^2\dfrac{\partial h}{\partial y}=gh\cos\alpha_y\sin\alpha_y \end{cases} , \tag{A1}$$

where h is the vertical water depth; u and v are the horizontal depth-averaged velocity components along the orthogonal directions x and y, respectively; g is the acceleration due to gravity; t is time; and α_x, α_y, and α_z are the angles between the corresponding axes of the local and global coordinate systems.

In the field of debris and mud flow modeling, assuming the two-phase mixture as an equivalent homogeneous fluid, Laigle (1997) proposed the following conservative formulation of the 2D depth-averaged equations:

$$\begin{cases} \dfrac{\partial h}{\partial t}+\dfrac{\partial (uh)}{\partial x}+\dfrac{\partial (vh)}{\partial y}=0 \\ \dfrac{\partial (uh)}{\partial t}+\dfrac{\partial }{\partial x}\left(u^2h+\dfrac{1}{2}\beta gh^2\right)+\dfrac{\partial }{\partial y}(uvh)=gh\sin\theta_x \\ \dfrac{\partial (vh)}{\partial t}+\dfrac{\partial }{\partial x}(uvh)+\dfrac{\partial }{\partial y}\left(v^2h+\dfrac{1}{2}\beta gh^2\right)=gh\sin\theta_y \end{cases} , \tag{A2}$$

in which h, u, and v are again the vertical flow depth and the depth-averaged velocity components in the x and y horizontal directions, respectively; θ_x and θ_y are the inclination angles of the bottom surface in the x- and y-directions, respectively; β is a reduction correction factor of the pressure term set to $\cos\theta_x \cos\theta_y$ without any physical explanation. Rickenmann et al. (2006) adopted the same set of equations in their 2D depth-averaged debris flow "HB" model (in which the moving mass is assumed to behave rheologically as a Herschel-Bulkley viscoplastic one-phase fluid). However, they assumed $\beta = \cos\theta_{xy}$, being θ_{xy} the "steepest slope angle" (Rickenmann et al., 2006; p. 247), which is presumably the local maximum bottom inclination angle.

Nakagawa and Takahashi (1997) modeled debris flow on steep bottom slopes using 2D depth-averaged equations that, for an unerodible bottom surface, reduce to (Takahashi, 2007, pp.158-159)

$$\begin{cases} \dfrac{\partial h}{\partial t}+\dfrac{\partial (uh)}{\partial x}+\dfrac{\partial (vh)}{\partial y}=0 \\ \dfrac{\partial (uh)}{\partial t}+\dfrac{\partial }{\partial x}(u^2h)+gh\cos\theta_x\dfrac{\partial h}{\partial x}+\dfrac{\partial }{\partial y}(uvh)=gh\sin\theta_x \\ \dfrac{\partial (vh)}{\partial t}+\dfrac{\partial }{\partial x}(uvh)+\dfrac{\partial }{\partial y}(v^2h)+gh\cos\theta_y\dfrac{\partial h}{\partial y}=gh\sin\theta_y \end{cases}, \tag{A3}$$

where different pressure correction factors are applied along the *x* and *y* directions in the momentum equations, even though it would be reasonable to expect that the same pressure correction factor appears in the two equations and that it is a symmetric function of the bottom inclination angles θ_x and θ_y (i.e. it remains unchanged as a result of the exchange of the coordinates *x* and *y*).

Another formulation of the 2D SSSWE was proposed by Denlinger and Iverson (2004), and Denlinger and O'Connel (2008) for the study of granular flows over irregular topographies. Adapting this model to a homogeneous fluid by assuming an isotropic stress tensor, the equations read

$$\begin{cases} \dfrac{\partial h}{\partial t}+\dfrac{\partial (uh)}{\partial x}+\dfrac{\partial (vh)}{\partial y}=0 \\ \dfrac{\partial (uh)}{\partial t}+\dfrac{\partial }{\partial x}\left(u^2h+\dfrac{1}{2}g'h^2\right)+\dfrac{\partial }{\partial y}(uvh)=g'h\dfrac{\partial b}{\partial x} \\ \dfrac{\partial (vh)}{\partial t}+\dfrac{\partial }{\partial x}(uvh)+\dfrac{\partial }{\partial y}\left(v^2h+\dfrac{1}{2}g'h^2\right)=g'h\dfrac{\partial b}{\partial y} \end{cases}, \tag{A4}$$

where *b* denotes the elevation of the bottom surface above a horizontal datum and *g'* is a total "enhanced" vertical acceleration defined as the sum of the acceleration due to gravity with the vertical acceleration of the fluid (see also Castro-Orgaz et al., 2015, p. 10; Castro-Orgaz and Hager, 2017, p. 41). The authors suggest assessing this latter quantity calculating the total derivative of the depth-averaged vertical velocity, which is estimated as the arithmetic average of the vertical velocities computed at the free surface and at the bottom by imposing the corresponding kinematic constraints (Denlinger and Iverson, 2004; pag. 4). However, numerical problems could arise at free surface discontinuities (such as at bores or at the initial discontinuity of a dam-break problem), where the vertical velocity is difficult to estimate because the water elevation gradient tends to infinite. Similarly, Juez et al. (2013), Xia and Liang (2018), and Ni et al. (2019) introduce in their 2D depth-averaged models in global coordinates a correction factor, ϕ, which reduces the gravity effect. This factor is assumed equal to the square cosine of the angle between the local normal to the bottom and the vertical direction, or the maximum bottom inclination angle (i.e. $\phi = 1/[1 + \tan^2\theta_x + \tan^2\theta_y]$).

In all previous formulations, the flow velocity components are assumed horizontal and the water depth is measured along the vertical direction, consistently with the use of a global horizontally-oriented coordinate system. Conversely, Iverson and Denlinger's (2001) formulation of the 2D depth-averaged equations for the description of the flow of grain-fluid mixtures on irregular topographies is based on the assumption that the water depth is measured perpendicularly to the bottom surface and the orthogonal velocity components are locally parallel to the bottom. Considering only normal fluid stresses as in fully liquefied inviscid masses, the equations proposed by Iverson and Denlinger (2001) become

$$\begin{cases} \dfrac{\partial \bar{h}}{\partial t}+\dfrac{\partial(\bar{u}\bar{h})}{\partial \xi}+\dfrac{\partial(\bar{v}\bar{h})}{\partial \eta}=0 \\ \dfrac{\partial(\bar{u}\bar{h})}{\partial t}+\dfrac{\partial}{\partial \xi}\left(\bar{u}^2\bar{h}\right)+g_\zeta \bar{h}\dfrac{\partial \bar{h}}{\partial \xi}+\dfrac{\partial}{\partial \eta}(\bar{u}\bar{v}\bar{h})=g_\xi \bar{h} \\ \dfrac{\partial(\bar{v}\bar{h})}{\partial t}+\dfrac{\partial}{\partial \xi}(\bar{u}\bar{v}\bar{h})+\dfrac{\partial}{\partial \eta}\left(\bar{v}^2\bar{h}\right)+g_\zeta \bar{h}\dfrac{\partial \bar{h}}{\partial \eta}=g_\eta \bar{h} \end{cases} , \tag{A5}$$

in which ξ and η denote orthogonal directions locally parallel to the bottom surface, and ζ is the axis normal to the bottom, while g_ξ, g_η, and g_ζ are the gravity acceleration components along ξ, η, and ζ directions, respectively. In Eq. (A5), the upper bar recalls that the flow variables are defined with respect to a bottom-oriented coordinate system. The same formulation of the equations in local coordinates was used by Juez et al. (2013) for granular flow modeling. Based on the same approach, McDougall and Hungr (2004) derived a set of governing equations written in non-conservative form to study the motion of landslides (assumed to behave as a homogeneous equivalent fluid of specified rheology). Neglecting entrainment of solid material due to erosion and the effects of the internal shear stresses, as well as bottom friction, these equations can be rewritten in conservative form as in Eq. (A5). However, the choice of defining the flow depth along the direction orthogonal to the bottom can cause modeling difficulties, especially on real topographies, as explained in Section 2.

Finally, describing a real-field application of the FLATModel numerical code, Medina et al. (2008) presented the basic 2D depth-averaged equations of the model which, neglecting the effect of flow curvature, are

$$\begin{cases} \dfrac{\partial \bar{h}}{\partial t}+\dfrac{\partial(\bar{u}\bar{h})}{\partial \xi}+\dfrac{\partial(\bar{v}\bar{h})}{\partial \eta}=0 \\ \dfrac{\partial(\bar{u}\bar{h})}{\partial t}+\dfrac{\partial}{\partial \xi}\left(\bar{u}^2\bar{h}+\dfrac{1}{2}g_p\bar{h}^2\right)+\dfrac{\partial}{\partial \eta}(\bar{u}\bar{v}\bar{h})=g_p\bar{h}\tan\theta_x \\ \dfrac{\partial(\bar{v}\bar{h})}{\partial t}+\dfrac{\partial}{\partial \xi}(\bar{u}\bar{v}\bar{h})+\dfrac{\partial}{\partial \eta}\left(\bar{v}^2\bar{h}+\dfrac{1}{2}g_p\bar{h}^2\right)=g_p\bar{h}\tan\theta_y \end{cases} , \tag{A6}$$

where $g_p = g\cos\theta$ denotes a corrected gravity acceleration, with θ being "the angle defined by the horizontal plane and the velocity direction" (Medina et al., 2008; p. 128). However, it seems unphysical that the correction factor depends on the local flow direction. Moreover, since flow depths are calculated along the vertical direction in the numerical code, geometrical transformations must be carried out at each time step in each computational cell, with negative impact on the computational efficiency.

Appendix B – Derivation of the governing equations

B.1 Continuity equation

Assuming incompressible flow, the rate of change of mass in the fixed control volume of Fig. 4 is

$$\rho\frac{\partial h}{\partial t}d\Omega\,, \tag{B1}$$

where ρ denotes the mass density. The flux of mass through the vertical trapezoidal face normal to x is

$$\rho(\mathbf{v}\cdot\hat{\mathbf{i}})hdy = \rho uh\cos\theta_x dy\,. \tag{B2}$$

Hence, the net influx of volume across the two opposite vertical faces normal to x is

$$-\rho\frac{\partial(uh\cos\theta_x)}{\partial x}d\Omega\,. \tag{B3}$$

Similarly, the net influx of volume across the two opposite vertical faces normal to y is

$$-\rho\frac{\partial(vh\cos\theta_y)}{\partial y}d\Omega\,. \tag{B4}$$

Therefore, equating the term in Eq. (B1) with the sum of the terms in Eqs (B3)–(B4) according to the mass conservation principle and dividing by ρdΩ, the following vertically-averaged continuity equation can be obtained:

$$\frac{\partial h}{\partial t}+\frac{\partial(uh\cos\theta_x)}{\partial x}+\frac{\partial(vh\cos\theta_y)}{\partial y}=0\,. \tag{B5}$$

B.2 Linear momentum equations

The linear momentum principle is applied to the fixed control volume shown in Fig. 4 along directions ξ and η. Only the derivation of the ξ-component equation is presented here. The equation in the η-direction can be obtained in a similar way.

Assuming incompressible flow, the rate of change of the ξ-momentum within the control volume is

$$\rho\frac{\partial}{\partial t}\left[(\mathbf{v}\cdot\hat{\boldsymbol{\xi}})h\right]d\Omega=\rho\frac{\partial(Uh)}{\partial t}d\Omega\,, \tag{B5}$$

where U is defined according to Eq. (6). The ξ-component of the net momentum flux entering the control volume through the opposite trapezoidal faces normal to x is

$$-\rho\frac{\partial}{\partial x}\left[(\mathbf{v}\cdot\hat{\boldsymbol{\xi}})(\mathbf{v}\cdot\hat{\mathbf{i}})h\right]d\Omega=-\rho\frac{\partial(uUh\cos\theta_x)}{\partial x}d\Omega\,, \tag{B6}$$

while the same quantity computed for the two opposite vertical faces normal to y is

$$-\rho\frac{\partial}{\partial y}\left[(\mathbf{v}\cdot\hat{\boldsymbol{\xi}})(\mathbf{v}\cdot\hat{\mathbf{j}})h\right]d\Omega=-\rho\frac{\partial(Uvh\cos\theta_y)}{\partial y}d\Omega\,. \tag{B7}$$

The total pressure force acting on the control surface in the ξ-direction is

$$-\rho\frac{\partial}{\partial x}\left[\frac{1}{2}kgh^2(\hat{\mathbf{i}}\cdot\hat{\boldsymbol{\xi}})\right]d\Omega=-\rho\left[\frac{1}{2}kgh^2\cos\theta_x\right]d\Omega\,, \tag{B8}$$

where g is the acceleration due to gravity and k is a dimensionless pressure correction factor ($k \le 1$). The ξ-component of the weight of the water enclosed in the control volume is

$$-\rho g(\hat{\mathbf{k}}\cdot\hat{\boldsymbol{\xi}})h\,d\Omega=\rho gh\sin\theta_x d\Omega\,, \tag{B9}$$

while, based on the 2D extension of the Manning formula (e.g. Molls et al., 1998), the component of the bed friction in the ξ-direction is

$$-\rho gh\frac{n^2u\|\mathbf{v}\|}{h^{4/3}}dA=-\rho gh\frac{n^2u\|\mathbf{v}\|}{h^{4/3}}d\Omega\sqrt{1+\tan^2\theta_x+\tan^2\theta_y}\,, \tag{B10}$$

where n is the Manning roughness coefficient. Combining the various terms according to the linear momentum principle and simplifying yields the vertically-averaged momentum equation in the ξ-direction:

$$\frac{\partial(Uh)}{\partial t}+\frac{\partial}{\partial x}\left[\left(uUh+\frac{1}{2}kgh^2\right)\cos\theta_x\right]+\frac{\partial}{\partial y}(Uvh\cos\theta_y)=gh\left(\sin\theta_x-\frac{n^2u\|\mathbf{v}\|}{h^{4/3}}\sqrt{1+\tan^2\theta_x+\tan^2\theta_y}\right). \tag{B11}$$

Similarly, the momentum equation in the η-direction is

$$\frac{\partial(Vh)}{\partial t}+\frac{\partial}{\partial x}(uVh\cos\theta_x)+\frac{\partial}{\partial y}\left[\left(vVh+\frac{1}{2}kgh^2\right)\cos\theta_y\right]=gh\left(\sin\theta_y-\frac{n^2v\|\mathbf{v}\|}{h^{4/3}}\sqrt{1+\tan^2\theta_x+\tan^2\theta_y}\right). \tag{B12}$$

Appendix C – Eigenstructure of the equations

Flux functions **F** and **G** defined in Eq. (15) must by explicitly expressed in terms of the conserved variables as

$$\mathbf{F}=\begin{bmatrix} (Uh-Vh\cos\varphi)\dfrac{\cos\theta_x}{\sin^2\varphi} \\ \left\{\dfrac{(Uh)^2-(Uh)(Vh)\cos\varphi}{h\sin^2\varphi}+\dfrac{1}{2}kgh^2\right\}\cos\theta_x \\ \dfrac{(Uh)(Vh)-(Vh)^2\cos\varphi}{h\sin^2\varphi}\cos\theta_x \end{bmatrix},\ \mathbf{G}=\begin{bmatrix} (Vh-Uh\cos\varphi)\dfrac{\cos\theta_y}{\sin^2\varphi} \\ \dfrac{(Uh)(Vh)-(Uh)^2\cos\varphi}{h\sin^2\varphi}\cos\theta_y \\ \left\{\dfrac{(Vh)^2-(Uh)(Vh)\cos\varphi}{h\sin^2\varphi}+\dfrac{1}{2}kgh^2\right\}\cos\theta_y \end{bmatrix}, \tag{C1}$$

where k is a factor that does not depend on the conserved variables.

The Jacobian matrices of flux functions **F** and **G** are respectively given by

$$\mathbf{J_F}=\begin{bmatrix} 0 & 1 & -\cos\varphi \\ -U^2+UV\cos\varphi+kgh\sin^2\varphi & 2U-V\cos\varphi & -U\cos\varphi_2 \\ -UV+V^2\cos\varphi & V & U-2V\cos\varphi \end{bmatrix}\frac{\cos\theta_x}{\sin^2\varphi} \tag{C2}$$

and

$$\mathbf{J_G}=\begin{bmatrix} 0 & -\cos\varphi & 1 \\ -UV+U^2\cos\varphi & V-2U\cos\varphi & U \\ -V^2+UV\cos\varphi+kgh\sin^2\varphi & -V\cos\varphi & 2V-U\cos\varphi \end{bmatrix}\frac{\cos\theta_y}{\sin^2\varphi}. \tag{C3}$$

The eigenvalues of $\mathbf{J_F}$ are

$$\lambda_{1,3}^{\mathbf{F}}=\left[U-V\cos\varphi\mp\sqrt{gh}\sqrt{k\sin^2\varphi}\right]\frac{\cos\theta_x}{\sin^2\varphi},\ \lambda_2^{\mathbf{F}}=(U-V\cos\varphi)\frac{\cos\theta_x}{\sin^2\varphi}, \tag{C4}$$

while the eigenvalues of $\mathbf{J_G}$ are

$$\lambda_{1,3}^{\mathbf{G}}=\left[V-U\cos\varphi\mp\sqrt{gh}\sqrt{k\sin^2\varphi}\right]\frac{\cos\theta_y}{\sin^2\varphi},\ \lambda_2^{\mathbf{G}}=(V-U\cos\varphi)\frac{\cos\theta_y}{\sin^2\varphi}. \tag{C5}$$

Eigenvalues $\lambda^{\mathbf{F}}$ and $\lambda^{\mathbf{G}}$ are real and distinct for $h \neq 0$, and the matrix defined as the linear combination of Jacobian matrices $\mathbf{J_F}$ and $\mathbf{J_G}$ has three distinct eigenvalues for $h \neq 0$, too. Therefore, the new equations are strictly hyperbolic for a wet bed (Toro, 2001; p. 39). Both Eqs (C2)–(C3) and Eqs (C4)–(C5) reduce to the well-known expressions valid for the conventional SWE when bottom slopes are small (Toro, 2001; pp. 32-33).

References

Acheson, D.J., 1990. Elementary Fluid Dynamics. Oxford University Press, Oxford, UK.

Ancey, C., Iverson, R.M., Rentschler, M., Denlinger, R.P., 2008. An exact solution for ideal dam-break floods on steep slopes. Water Resour. Res. 44(1), W01430. https://doi.org/10.1029/2007WR006353.

Antuono, M., Hogg, A.J., 2009. Run-up and backwash bore formation from dam-break flow on an inclined plane. J. Fluid Mech. 640, 151–164.

https://doi.org/10.1017/S0022112009991698.

Aureli, F., Dazzi, S., Maranzoni, A., Mignosa, P., Vacondio, R., 2015. Experimental and numerical evaluation of the force due to the impact of a dam-break wave on a structure. Adv. Water Resour., 76, 29–42. https://doi.org/10.1016/j.advwatres.2014.11.009.

Aureli, F., Maranzoni, A., Mignosa, P., 2014. A semi-analytical method for predicting the outflow hydrograph due to dam-break in natural valleys. Adv. Water Resour. 63, 38–44. https://doi.org/10.1016/j.advwatres.2013.11.001.

Aureli, A., Maranzoni, A., Mignosa, P., Ziveri, C., 2006. Flood hazard mapping by means of fully-2D and quasi-2D numerical modeling: a case study. In Floods, from defence to management, van Alphen, J., van Beek, E., and Taal, M. eds. 3rd International Symposium on Flood Defence, Nijmegen, Netherlands, Taylor & Francis/Balkema, pp. 373–382.

Aureli, F., Maranzoni, A., Mignosa, P., Ziveri, C., 2008. A weighted surface-depth gradient method for the numerical integration of the 2D shallow water equations with topography. Adv. Water Resour. 31(7), 962–974. https://doi.org/10.1016/j.advwatres.2008.03.005.

Barbolini, M., Gruber, U., Keylock, C.J., Naaim, M., Savi, F., 2000. Application of statistical and hydraulic-continuum dense-snow avalanche models to five real European sites. Cold Reg. Sci. Technol. 31(2), 133–149. https://doi.org/10.1016/S0165-232X(00)00008-2.

Basco, D.R., 1989. Limitations of de Saint Venant equations in dam-break analysis. J. Hydraul. Eng. 115(7), 950–965. https://doi.org/10.1061/(ASCE)0733-9429(1989)115:7(950).

Begnudelli, L., Sanders, B.F., 2007. Simulation of the St. Francis dam-break flood. J. Eng. Mech. 133(11), 1200–1212. https://doi.org/10.1061/(ASCE)0733-9399(2007)133:11(1200).

Berger, R.C., 1994. Strengths and weaknesses of shallow water equations in steep open channel flow. Hydraulic Engineering, G.V. Cotroneo and R.R. Rumer eds., ASCE, New York, NY, pp. 1257–1262.

Cantero-Chinchilla, F.N., Bergillos, R.J., Gamero, P., Castro-Orgaz, O., Cea, L., Hager, W.H., 2020. Vertically averaged and moment equations for dam-break wave modeling: Shallow water hypotheses. Water 12(11), 3232. https://doi.org/10.3390/w12113232.

Cantero-Chinchilla, F.N., Castro-Orgaz, O., Dey, S., Ayuso, J.L., 2016. Nonhydrostatic dam break flows. I: Physical equations and numerical schemes. J. Hydraul. Eng. 142(12), 04016068. https://doi.org/10.1061/(ASCE)HY.1943-7900.0001205.

Castro-Orgaz, O., Hager, W.H., 2014. One-dimensional modelling of curvilinear free surface flow: generalized Matthew theory. J. Hydraul. Res. 52(1), 14–23. https://doi.org/10.1080/00221686.2013.834853.

Castro-Orgaz, O., Hager, W.H., 2016. Dressler's theory for curved topography flows: iterative derivation, transcritical flow solutions and higher-order wave-type equations. Environ. Fluid Mech. 16(2), 289–311. https://doi.org/10.1007/s10652-015-9418-z.

Castro-Orgaz, O., Hager, W.H., 2017. Non-Hydrostatic Free Surface Flows. Springer, Cham, Switzerland.

Castro-Orgaz, O., Hutter, K., Giraldez, J.V., Hager, W.H., 2015. Nonhydrostatic granular flow over 3-D terrain: New Boussinesq-type gravity waves? J. Geophys. Res. Earth. Surf. 120(1), 1–28. https://doi.org/10.1002/2014JF003279.

Cea, L., Bladé, E., 2015. A simple and efficient unstructured finite volume scheme for solving the shallow water equations in overland flow applications. Water Resour. Res. 51(7), 5464–5486. https://doi.org/10.1002/2014WR016547.

Cea, L., López-Núñez, A., 2021. Extension of the two-component pressure approach for modeling mixed free-surface-pressurized flows with the two-dimensional shallow water equations. Int. J. Numer. Methods Fluids 93(3), 628–652. https://doi.org/10.1002/fld.4902.

Chaudhry, M.H., 1993. Open-Channel Flow. Prentice-Hall, Englewood Cliffs, NJ.

Chow, V.T., 1959. Open-Channel Hydraulics. McGraw-Hill, New York, NY.

Christen, M., Kowalski, J., Bartelt, P., 2010. RAMMS: Numerical simulation of dense snow avalanches in three-dimensional terrain. Cold Reg. Sci. Technol. 63(1–2), 1–14. https://doi.org/10.1016/j.coldregions.2010.04.005.

Costabile, P., Costanzo, C., Ferraro, D., Macchione, F., Petaccia, G., 2020. Performances of the new HEC-RAS version 5 for 2-D hydrodynamic-based rainfall-runoff simulations at basin scale: Comparison with a state-of-the art model. Water 12(9), 2326. https://doi.org/10.3390/w12092326.

Dazzi, S., Vacondio, R., Mignosa, P., 2019. Integration of a levee breach erosion model in a GPU-accelerated 2D shallow water equations code. Water Resour. Res. 55(1), 682–702. https://doi.org/10.1029/2018WR023826.

de Almeida, G.A., Bates, P., Freer, J.E., Souvignet, M., 2012. Improving the stability of a simple formulation of the shallow water equations for 2-D flood modeling. Water Resour. Res. 48(5), W05528. https://doi.org/10.1029/2011WR011570.

Denlinger, R.P., Iverson, R.M., 2004. Granular avalanches across irregular three-dimensional terrain: 1. Theory and computation. J. Geophys. Res.-Earth 109, F01014. https://doi.org/10.1029/2003JF000085.

Denlinger, R.P., O'Connell, D.R., 2008. Computing nonhydrostatic shallow-water flow over steep terrain. J. Hydraul. Eng. 134(11), 1590–1602. https://doi.org/10.1061/(ASCE)0733-9429(2008)134:11(1590).

D'Oria, M., Maranzoni, A., Mazzoleni, M., 2019. Probabilistic assessment of flood hazard due to levee breaches using fragility functions. Water Resour. Res. 55(11), 8740–8764. https://doi.org/10.1029/2019WR025369.

Dressler, R.F., 1958. Unsteady non-linear waves in sloping channels. Proc. R. Soc. Lond. A 247(1249), 186–198. https://doi.org/10.1098/rspa.1958.0177.

Dressler, R.F., 1978. New nonlinear shallow-flow equations with curvature. J. Hydraul. Res. 16(3), 205–222. https://doi.org/10.1080/00221687809499617.

Fabiani, A.L.T., Ota, J.J., 2019. Two-dimensional Boussinesq equations applied to channel flows: deducing and applying the equations. Rev. Bras. Recur. Hidr. 24, e25. https://doi.org/10.1590/2318-0331.241920180159.

Fernandez-Feria, R., 2006. Dam-break flow for arbitrary slopes of the bottom. J. Eng. Math. 54(4), 319–331. https://doi.org/10.1007/s10665-006-9034-5.

Gray, J.M.N.T., Wieland, M., Hutter, K., 1999. Gravity-driven free surface flow of granular avalanches over complex basal topography. Proc. R. Soc. Lond. A 455(1985), 1841–1874. https://doi.org/10.1098/rspa.1999.0383.

Gruber, U., Bartelt, P., 2007. Snow avalanche hazard modelling of large areas using shallow

water numerical methods and GIS. Environ. Model. Softw. 22(10), 1472–1481. https://doi.org/10.1016/j.envsoft.2007.01.001.

Guinot, V., Cappelaere, B., 2009. Sensitivity analysis of 2D steady-state shallow water flow. Application to free surface flow model calibration. Adv. Water Res. 32(4), 540–560. https://doi.org/10.1016/j.advwatres.2009.01.005.

Han, G., Wang, D., 1996. Numerical modeling of Anhui debris flow. J. Hydraul. Eng. 122(5), 262–265. https://doi.org/10.1061/(ASCE)0733-9429(1996)122:5(262).

Henderson, F.M., 1966. Open Channel Flow. Prentice-Hall, Upper Saddle River, NJ.

Horna-Munoz, D., Constantinescu, G., 2020. 3-D dam break flow simulations in simplified and complex domains. Adv. Water Resour. 137, 103510. https://doi.org/10.1016/j.advwatres.2020.103510.

Horritt, M.S., Bates, P.D., 2002. Evaluation of 1D and 2D numerical models for predicting river flood inundation. J. Hydrol. 268(1–4), 87–99. https://doi.org/10.1016/S0022-1694(02)00121-X.

Hu, K., Meyer, D., 2005. The validity of the non-linear shallow water equations for modelling wave runup and reflection. In International Conference on Coastlines, structures and breakwaters 2005 (pp. 195–206). Thomas Telford Publishing, UK.

Hunt, B., 1987. An inviscid dam-break solution. J. Hydraul. Res. 25(3), 313–327. https://doi.org/10.1080/00221688709499273.

Iverson, R.M., Denlinger, R.P., 2001. Flow of variably fluidized granular masses across three-dimensional terrain: 1. Coulomb mixture theory. J. Geophys. Res-Sol. Ea. 106(B1), 537–552. https://doi.org/10.1029/2000JB900329.

Juez, C., Murillo, J., García-Navarro, P., 2013. 2D simulation of granular flow over irregular steep slopes using global and local coordinates. J. Comput. Phys. 255, 166–204. http://dx.doi.org/10.1016/j.jcp.2013.08.002.

Keller, J.B., 2003. Shallow-water theory for arbitrary slopes of the bottom. J. Fluid Mech. 489, 345–348. https://doi.org/10.1017/S0022112003005342.

Kim, D.H., Lynett, P.J., 2011. Dispersive and nonhydrostatic pressure effects at the front of surge. J. Hydraul. Eng. 137(7), 754–765. https://doi.org/10.1061/(ASCE)HY.1943-7900.0000345.

Laigle, D., 1997. A two-dimensional model for the study of debris-flow spreading on a torrent debris fan. Debris-Flow Hazards Mitigation: Mechanics, Prediction, and Assessment, C. Chen ed., ASCE, New York, NY, pp. 123–132.

Laigle, D., Coussot, P., 1997. Numerical modeling of mudflows. J. Hydraul. Eng. 123(7), 617–623. https://doi.org/10.1061/(ASCE)0733-9429(1997)123:7(617).

LeVeque, R.J., George, D.L., Berger, M.J., 2011. Tsunami modelling with adaptively refined finite volume methods. Acta Numer. 20, 211–289. https://doi.org/10.1017/S0962492911000043.

Mancarella, D., Hungr, O., 2010. Analysis of run-up of granular avalanches against steep, adverse slopes and protective barriers. Can. Geotech. J. 47(8), 827–841. https://doi.org/10.1139/T09-143.

Mangeney-Castelnau, A., Bouchut, F., Vilotte, J. P., Lajeunesse, E., Aubertin, A., Pirulli, M.,

2005. On the use of Saint Venant equations to simulate the spreading of a granular mass. J. Geophys. Res. Solid Earth 110(B9), B09103. https://doi.org/10.1029/2004JB003161.

Maranzoni, A., Dazzi, S., Aureli, F., Mignosa, P., 2015. Extension and application of the Preissmann slot model to 2D transient mixed flows. Adv. Water Resour. 82, 70–82. https://doi.org/10.1016/j.advwatres.2015.04.010.

Maranzoni, A., Mignosa, P., 2018. Numerical treatment of a discontinuous top surface in 2D shallow water mixed flow modeling. Int. J. Numer. Methods Fluids 86(4), 290–311. https://doi.org/10.1002/fld.4418.

Maranzoni, A., Mignosa, P., 2019. Seismic-generated unsteady motions in shallow basins and channels. Part I: Smooth analytical solutions. Appl. Math. Model. 68, 696–711. https://doi.org/10.1016/j.apm.2018.07.046.

Maranzoni, A., Tomirotti, M., 2021. New formulation of the two-dimensional steep-slope shallow water equations. Part II: Numerical modeling, validation and application. Adv. Water Res. (companion paper).

McDougall, S., Hungr, O., 2004. A model for the analysis of rapid landslide motion across three-dimensional terrain. Can. Geotech. J. 41(6), 1084–1097. https://doi.org/10.1139/t04-052.

Medina, V., Hürlimann, M., Bateman, A., 2008. Application of FLATModel, a 2D finite volume code, to debris flows in the northeastern part of the Iberian Peninsula. Landslides 5(1), 127–142. https://doi.org/10.1007/s10346-007-0102-3.

Mohapatra, P.K., Chaudhry, M.H., 2004. Numerical solution of Boussinesq equations to simulate dam-break flows. J. Hydraul. Eng. 130(2), 156–159. https://doi.org/10.1061/(ASCE)0733-9429(2004)130:2(156).

Molls, T., Zhao, G., Molls, F., 1998. Friction slope in depth-averaged flow. J. Hydraul. Eng. 124(1), 81–85. https://doi.org/10.1061/(ASCE)0733-9429(1998)124:1(81).

Nakagawa, H., Takahashi, T., 1997. Estimation of a debris flow hydrograph and hazard area. Debris-Flow Hazards Mitigation: Mechanics, Prediction, and Assessment, C. Chen ed., ASCE, New York, NY, pp. 64–73.

Ni, Y., Cao, Z., Liu, Q., 2019. Mathematical modeling of shallow-water flows on steep slopes. J. Hydrol. Hydromech. 67(3), 252–259. https://doi.org/10.2478/johh-2019-0012.

O'Brien, J.S., Julien, P.Y., Fullerton, W.T., 1993. Two-dimensional water flood and mudflow simulation. J. Hydraul. Eng. 119(2), 244–261. https://doi.org/10.1061/(ASCE)0733-9429(1993)119:2(244).

Pan, C.H., Lin, B.Y., Mao, X.Z., 2007. Case study: Numerical modeling of the tidal bore on the Qiantang River, China. J. Hydraul. Eng. 133(2), 130–138. https://doi.org/10.1061/(ASCE)0733-9429(2007)133:2(130).

Petaccia, G., Natale, L., 2020. 1935 Sella Zerbino dam-break case revisited: A new hydrologic and hydraulic analysis. J. Hydraul. Eng. 146(8), 05020005. https://doi.org/10.1061/(ASCE)HY.1943-7900.0001760.

Pilotti, M., Maranzoni, A., Milanesi, L., Tomirotti, M., Valerio, G., 2014. Dam-break modeling in alpine valleys. J. Mt. Sci. 11(6), 1429–1441. https://doi.org/10.1007/s11629-014-3042-0.

Pilotti, M., Maranzoni, A., Tomirotti, M., Valerio, G., 2011. 1923 Gleno dam break: Case

study and numerical modeling. J. Hydraul. Eng. 137(4), 480–492. https://doi.org/10.1061/(ASCE)HY.1943-7900.0000327.

Pilotti, M., Milanesi, L., Bacchi, V., Tomirotti, M., Maranzoni, A., 2020. Dam-break wave propagation in an alpine valley with HEC-RAS 2D: the experimental Cancano test case. J. Hydraul. Eng. 146(6), 05020003. https://doi.org/10.1061/(ASCE)HY.1943-7900.0001779.

Rickenmann, D., Laigle, D., McArdell, B.W., Hübl, J., 2006. Comparison of 2D debris-flow simulation models with field events. Comput. Geosci. 10(2), 241–264. https://doi.org/10.1007/s10596-005-9021-3.

Savage, S.B., & Hutter, K., 1989. The motion of a finite mass of granular material down a rough incline. J. Fluid Mech. 199, 177–215. https://doi.org/10.1017/S0022112089000340.

Segur, H., 2007. Waves in shallow water, with emphasis on the tsunami of 2004. In: Tsunami and nonlinear waves (pp. 3–29). Springer, Berlin, Germany.

Sharma, V.C., Regonda, S.K., 2021. Two-dimensional flood inundation modeling in the Godavari River basin, India – Insights on model output uncertainty. Water 13(2), 191. https://doi.org/10.3390/w13020191.

Singh, J., Altinakar, M.S., Ding, Y., 2015. Numerical modeling of rainfall-generated overland flow using nonlinear shallow-water equations. J. Hydrol. Eng. 20(8), 04014089. https://doi.org/10.1061/(ASCE)HE.1943-5584.0001124.

Sivakumaran, N.S., Dressler, R.F., 1989. Unsteady density-current equations for highly curved terrain. J. Atmos. Sci. 46(20), 3192–3201. https://doi.org/10.1175/1520-0469(1989)046<3192:UDCEFH>2.0.CO;2.

Takahashi, T., 2007. Debris Flow. Mechanics, Prediction and Countermeasures. 1st Ed. Taylor & Francis, London, UK.

Teng, J., Jakeman, A.J., Vaze, J., Croke, B.F., Dutta, D., Kim, S., 2017. Flood inundation modelling: A review of methods, recent advances and uncertainty analysis. Environ. Model. Softw. 90, 201–216. https://doi.org/10.1016/j.envsoft.2017.01.006.

Toro, E.F., 2001. Shock-Capturing Methods for Free-Surface Shallow Flows. John Wiley & Sons, Chichester, UK.

Touma, R., Kanbar, F, 2018. Well-balanced central schemes for two-dimensional systems of shallow water equations with wet and dry states. Appl. Math. Model. 62, 728–750. https://doi.org/10.1016/j.apm.2018.06.032.

Valiani, A., Caleffi, V., Zanni, A., 2002. Case study: Malpasset dam-break simulation using a two-dimensional finite volume method. J. Hydraul. Eng. 128(5), 460–472. https://doi.org/10.1061/(ASCE)0733-9429(2002)128:5(460).

Van Emelen, S., Zech, Y., Soares-Frazão, S., 2014. Limitations of the shallow water assumptions for problems involving steep slopes: Application to a dike overtopping test case. In River Flow 2014, Schleiss, A.J., De Cesare, G., Franca, M.J., Pfister, M. eds. International Conference on Fluvial Hydraulics, Lausanne, Switzerland, CRC Press.

Viero, D.P., D'Alpaos, A., Carniello, L., & Defina, A., 2013. Mathematical modeling of flooding due to river bank failure. Adv. Water Res. 59, 82–94. https://doi.org/10.1016/j.advwatres.2013.05.011.

Wang, Y., Liang, Q., Kesserwani, G., Hall, J.W., 2011. A 2D shallow flow model for practical dam-break simulations. J. Hydraul. Res. 49(3), 307–316.

https://doi.org/10.1080/00221686.2011.566248.

Xia, J., Falconer, R.A., Lin, B., Tan, G., 2011. Numerical assessment of flood hazard risk to people and vehicles in flash floods. Environ. Model. Softw. 26(8), 987–998. https://doi.org/10.1016/j.envsoft.2011.02.017.

Xia, X., Liang, Q., 2018. A new depth-averaged model for flow-like landslides over complex terrains with curvatures and steep slopes. Eng. Geol. 234, 174–191. https://doi.org/10.1016/j.enggeo.2018.01.011.

Zischg, A.P., Felder, G., Mosimann, M., Röthlisberger, V., Weingartner, R., 2018. Extending coupled hydrological-hydraulic model chains with a surrogate model for the estimation of flood losses. Environ. Model. Softw. 108, 174–185. https://doi.org/10.1016/j.envsoft.2018.08.009.

List of figure captions

Fig. 1. Example of a difficulty that can be encountered in 1D dam-break modeling in a sloping channel considering bottom-normal flow depths: segment AA' intersects the dam (and not the water surface) and does not define correctly a water depth measured perpendicularly from the bottom.

Fig. 2. Example of geometrical difficulties caused by a curved bottom: lines AA' and BB' traced orthogonally to the bottom intersect.

Fig. 3. Definition sketch of free-surface flow on a steep bottom surface: (a) 3D view; (b) profile view on the *yz* vertical plane.

Fig. 4. Infinitesimal control volume used for the derivation of the 2D vertically-averaged equations.

Fig. 5. 1D dam-break problem in a sloping channel with fixed bottom slope: initial condition (at time $t_0 = 0$) and water surface profile at generic time $t > 0$.

Fig. 6. Dam-break on a steep frictionless channel with fixed slope: (a) analytical solutions for the quiet front, drying front, and wetting front in the dimensionless characteristic plane; (b) comparison between the analytical solutions of the quiet, drying, and wetting fronts for the SSSWE and SWE models for $\theta_x = 45°$ and $h_0 = 1$ m. t_e denotes the empting time of the reservoir.